SUPPLEMENTARY INFORMATION

Differential copper-guided architectures of amyloid β peptidomimetics modulate oxidation states and catalysis

Debasis Ghosh[a], Mouli Konar[a], Tanmay Mondal[a] and Thimmaiah Govindaraju*[a]

[a] Debasis Ghosh, Mouli Konar, Tanmay Mondal, Prof. T. Govindaraju

Bioorganic Chemistry Laboratory, New Chemistry Unit and School of Advanced Materials (SAMat),

Jawaharlal Nehru Centre for Advanced Scientific Research, Jakkur P.O., Bengaluru 560064, Karnataka, India.

E-mail: tgraju@jncasr.ac.in

Table of Contents

1. General methods

All the peptides and peptidomimetics are synthesized by standard solid phase peptide synthesis (SPPS) protocols. Fmoc-rink amide resin (Novabiochem) was used as solid support. Amino acids and unnatural CDP-amino acid (kd) were coupled using HBTU/HOBt as the activating reagent, DIPEA as the base in DMF. For deprotection of the Fmoc protecting group, 20% piperidine in DMF was used. All peptides were purified using reverse-phase (RP) semi-preparative HPLC using a C18 column at 40 °C. The product purity was >99%, as ascertained by the analytical HPLC. The molecular mass of peptides was verified by HRMS (Q-TOF) analysis. The sequence and structural information of synthesized kd-incorporated peptidomimetics are given in Table S5.

1.1 Synthesis of Aβ14-23, Aβ14-23Py, Akd^{NMC}, Akd^{NMC}Py and HkdPy peptidomimetics

The unnatural CDP amino acid (kd) was synthesized by cyclizing Fmoc-Asp(O^{t}Bu)-OH and H-Lys(Boc)-OMe.[1,2] We used standard 9-fluorenylmethoxycarbonyl (Fmoc) SPPS protocols to synthesize kd-incorporated peptidomimetics. Fmoc-amino acids (H: Histidine, Q: Glutamine, K: Lysine, L: Leucine, V: Valine, F: Phenylalanine, A: Alanine, E: Glutamic acid, D: Aspartic acid, and Py: Pyrene acetic acid) with the Boc and ^{t}Bu protected side chains of the corresponding -NH_2 and -COOH functions were employed. The rink amide resin (loading 0.76 mmol/gm) was used as solid support. HBTU/HOBt (2.5 eq. each), DIPEA (4 eq.), and DMF were employed as activating reagent, base and solvent, respectively, for coupling the Fmoc-amino acids (2.5 eq.) and the Fmoc-kd (2.5 eq.) in the desired sequence. In the final step, 2.5 eq of 1-pyrene acetic acid (Py) was conjugated to the N-terminus. Kaiser test was used to ensure that the amino acid's coupling and Fmoc-deprotection processes were completed. The resin was properly washed with DMF and DCM after each coupling and deprotection procedure. Using a cocktail solution of TFA: TIPS: DCM (95:2.5:2.5) at room temperature, the entire sequence of the peptidomimetics was cleaved from the resin and the product was collected as solid precipitate from the cold diethyl-ether. Reverse-phase HPLC was used to purify the synthesized peptidomimetics (C18 column).

1.2 Preparation of the peptide stock solution

Purified lyophilized peptides were dissolved in water (Mili-Q) to make a 1 mM stock solution.

1.3 Metal binding study

The binding and selectivity of $Akd^{NMC}Py$ (15 μM) peptide toward various metal ions, e.g. Al^{III}, Cu^{II}, Zn^{II}, Fe^{II} and Fe^{III} were evaluated by absorbance and fluorescence studies. A 6.5-fold higher concentration of metal ions (100 μM) was used during the sample preparation, Cu^{II}, Fe^{II} and Fe^{III} were found to bind efficiently to $Akd^{NMC}Py$, as confirmed by the significant change in fluorescence of $Akd^{NMC}Py$.

1.4 Atomic force microscopy (AFM) characterization

The AFM imaging was performed for $Akd^{NMC}Py$, and one-off addition $Akd^{NMC}Py+Cu^{II}$ samples. 10 μL of 5 μM aliquot was drop-casted onto freshly cleaved mica and incubated for 5 min, followed by rinsing with water (Milli-Q) and dried by the flow of air. The AFM images were acquired using Bruker BIOSCOPE Resolve with PeakForce Tapping mode. The silicon Tip on the Nitride Lever (SCANASYST-AIR) was used. The length, radius and resonance frequency of the tip is 115 μm, 5 nm and 70 kHz, respectively; and the force constant is 0.4 Nm^{-1}. All the images were processed using NanoScope analysis software 1.8.

1.5 Kinetic assay with fluorescein (DCFHDA) derivatives

Kinetics measurements were carried out in 96-well plates using SpectraMax i3x microplate reader (Molecular Devices), by monitoring the absorbance of the product generated (DCF, 2',7'-dichlorofluorescein) at 504 nm at 37 °C. DCFH-DA (Sigma Aldrich) was dissolved in DMSO to obtain a stock solution (10 mM). Varying concentrations of substrate (DCFH-DA) including 100 μM, 500 μM, 1 mM, 2 mM, and 2.5 mM were used in the assays. The concentration of metal-peptide utilized in the studies was 2 μM. The absorbance of DCF generated was measured after mixing with $Akd^{NMC}Py+Cu^{II}$ complex. The studies were carried out in HEPES buffer (25 mM, pH 8). For the kinetics investigation, the control sample (negative control) was considered during the experiment, e.g. only Cu^{II}, $Akd^{NMC}Py$, Akd^{NMC}, Aβ14-23, Aβ14-23Py and HkdPy. The linear portion of the absorbance vs. time plot was fitted to a linear equation and the initial rate of the reaction was calculated using slope/extinction coefficient of the product at pH 8 (90,750 $M^{-1}cm^{-1}$). Kinetic parameters were obtained by fitting the data to the Michaelis–Menten equation $V_0 = k_{cat}[E]_0[S]_0/(KM+[S]_0)$, K_{cat} calculated from $V_{max}/(E)$, and catalytic efficiency was calculated from K_{cat}/K_M (Turnover number).

1.6 Cyclic voltammetry (CV) experiment

The electrochemical experiments were performed using CHI 832 electrochemical workstation (CH Instruments, Austin, Texas). Cyclic voltammograms were obtained at room temperature, nitrogen gas was purged into the electrolyte solution. The saturated calomel electrode was used as a reference electrode, platinum coil as a counter electrode and platinum disk as a working electrode. The redox behaviour of the Cu^{II} (copper nitrate) was carried out in 0.2 M KCl. It had been observed that electroactive Cu^{II} solution gives two cathodic peaks and an anodic peak. The first cathodic peak current was at -8.6 µA and potential 0.034 V, and the second peak was at -1.35 µA and potential -0.128 V. The anodic peak current was 33.5 µA and the potential 0.124 V. This implied the two-electron reversible system. In the presence of $Akd^{NMC}Py$ the current density decreased due to binding $Akd^{NMC}Py$ with Cu^{II}. In the presence of $Akd^{NMC}Py$, only an anodic positive peak at 0.015 V and another at 0.27 V were observed. More importantly, the reduction peak becomes less significant, which provided information about the redox state of copper in the presence $Akd^{NMC}Py$.

1.7 Transmission electron microscopy (TEM) characterization

5 µL of the sample was placed onto a carbon-coated copper grid and dried completely. Then 2 µL of 2 % (w/v) uranyl acetate solution was added for 45 sec and excess solution was wicked off by filter paper. Sample concentrations were typically 10-15 µM in 10 mM PBS. The specimen was observed using JEOL-JEM 2010 instrument operating at 120 kV and the image was recorded with SC 1000 CCD camera (Gatan). The data were analyzed using Digital Micrograph software.

1.8 Fourier-Transform Infrared Spectroscopy (FTIR)

FTIR spectra were recorded on Frontier (model: Sr No. 96466) spectrometer and in ATR mode. The aqueous solution of each sample (20 µL) was drop-casted on the thin coverslip, and then the sample was dried at room temperature under high vacuum. During the experiment, the scan rate was kept around 60 min s^{-1}. The baseline correction for each recorded sample was performed by the instrument inbuild software. The final data were plotted using the Origin software.

1.9 Field emission scanning electron microscopy (FESEM)

FESEM images were acquired using FEI Nove-nano SEM-600 equipped with a gun operating with the voltage 10.00 kV. The sample was prepared by drop-casting on a Si-wafer (111) substrate. The $Akd^{NMC}Py$-Cu^{II} complexes showed two distinct nanoarchitectures formations depending on the modes of addition of Cu^{II} (one-off or serial addition). In the serial addition mode, we found

micelle-like core-shell architectures and in one-off addition resulted in the formation of 2D nanosheets.

1.10 Circular dichroism (CD) spectroscopy

CD measurements were carried out on Jasco J-815 spectrometer under a nitrogen atmosphere to avoid water condensation. Scans were performed with the sample in 1 cm quartz cell over the range of 195–600 nm with a scan speed of 100 nm/min, and the spectra represent an average of three scans. A blank sample containing PBS buffer (10 mM, pH = 7.4) was treated in the same manner and subtracted from the collected data. Interestingly, in the case of serial addition, we observed a negative cotton effect at 298 nm. With increasing concentration of Cu^{II} the band at 298 showed an enhanced negative cotton effect.

1.11 Electronic paramagnetic resonance (EPR)

Aqueous solution of Cu^{II} (1 mM, 75 μL) and peptide stock solution (1 mM) were mixed. The mixture was diluted in PBS (10 mM, pH 7.4). The mixture was incubated at room temperature for 2 h. The sample was transferred into an EPR tube and flash-frozen in liquid nitrogen. The EPR spectra were recorded in a time-dependent manner in Wilmad tube using a JEOL, JES-X320 EPR spectrometer by considering g^{II} and A^{II} values for Cu^{II}.

1.12 Molecular docking

$Akd^{NMC}Py$ peptidomimetic was docked with $Akd^{NMC}Py$-Cu by using AutoDock Vina (version 1.1.2) software. The PDB format of $Akd^{NMC}Py$ was generated by OpenBabel software (version 2.4.1) after minimizing energy. AutoDock 4.2 MGL Tools (version 1.5.6) was applied for the preparation of $Akd^{NMC}Py$-Cu (here as a receptor), where to predict binding mode more accurately, water molecules were eliminated, polar hydrogen atoms were added to it to find plausible polar contacts with any atom, gasteiger charges of the peptidomimetics were included and saved as pdbqt format. Also, the pdbqt format of $Akd^{NMC}Py$ was created to coordinate files, which consist of atomic partial charges and atom types. Torsion angles were determined to consign the fixable and non-bonded rotation of molecules. The grid file, modified to calculate the grid parameters, is an imaginary box of customized volume so that $Akd^{NMC}Py$ can bind to the best reasonable binding site with the lowest binding energy and with higher binding affinity. We performed a blind docking experiment of $Akd^{NMC}Py$ with grid volume of 84 x 84 x 84 points, grid spacing of 0.503 Å and centred (-0.671 for x-axis, -6.274 for y-axis, and -16.394 for z-axis) on the receptor $Akd^{NMC}Py$-

Cu. At the end of the experiment, the output file was produced as ligand_out.pdbqt which includes binding affinity (-5.4 in kcal/mol), RMSD lb and RMSD ub. PyMOL software (version 1.7.4.5) was used to analyze the results of molecular docking. The hydrophobic residues were selected and labelled as required.

1.13 DFT calculation

From the most stable conformation of Akd^{NMC}Py-Cu^{II} (Fig. S9), calculated by DFT (B3LYP, 6-31G), it was evident that Cu^{II} was coordinated by ^{14}His (1.3 Å), ^{22}Glu (3.9 Å), ^{23}Asp (3.2 Å), and C-terminus kd (4.0 Å, N-terminus kd 5.5 Å); and aromatic interactions play a crucial role to form the zipper structure where pyrene was 6.6 Å apart from Cu^{II}. Based on the statistical analysis on the PDB, the RING server classified various interaction types, among which the strict and relaxed distance for the pi-cation interaction were reported as 5 Å and 7 Å respectively. Besides parallel, lateral and normal orientations, a peak around 6.2 Å was found for the orthogonal (N) conformation, corresponding to a situation where the charged group is placed opposite to the interacting ring.[3] Further, π-π aromatic interactions support in favour of thermodynamically stable sheet architecture. The density functional theory (DFT) was calculated by Gaussian 5.0.9 program to get the most stable conformation of copper bound Akd^{NMC}Py. Herein, B3LYP was used as an energy functional and 6-31G as a basis set.

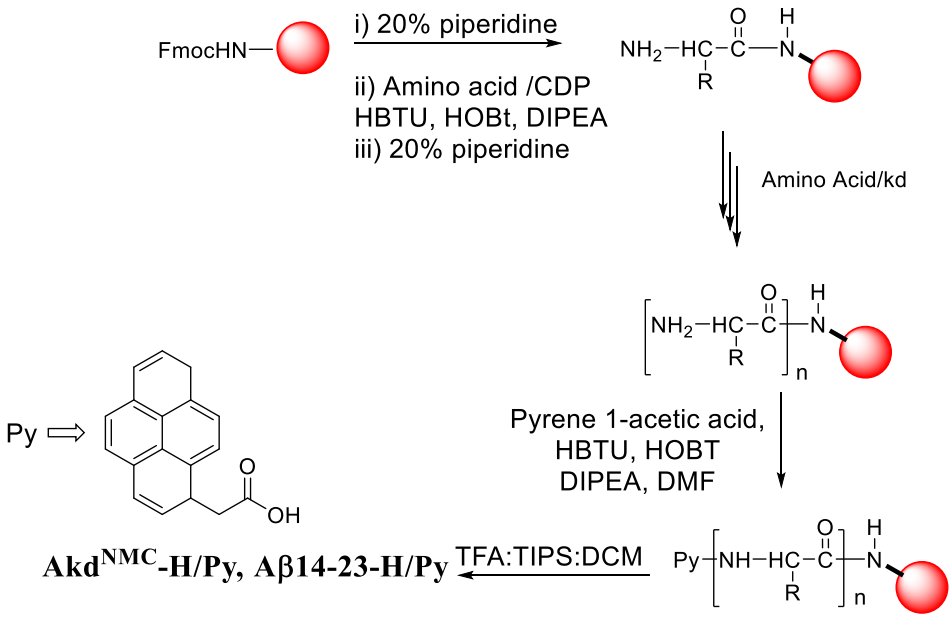

Fig. S1 A general SPPS scheme for the synthesis of peptide and peptidomimetics.

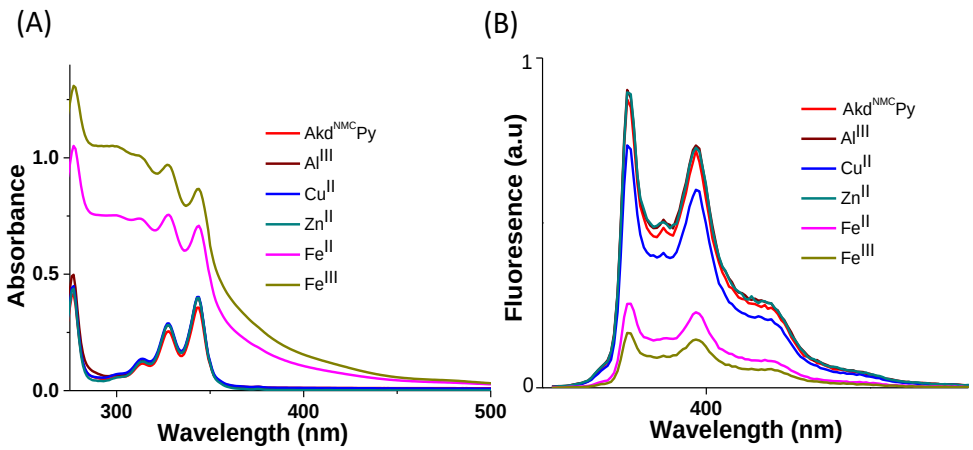

Fig. S2 Akd^{NMC}Py to various metal ions. (A) Absorbance spectra of Akd^{NMC}Py (15 M) and in the presence of metal ions 25 °C in PBS buffer (10 mM, pH 7.4). (B) Fluorescence spectra of Akd^{NMC}Py and in the presence of metal ions at 25 °C in PBS buffer (10 mM, pH 7.4) at the excitation wavelength λ_{ex} = 343 nm. [Metal ion] =100 μM, [Akd^{NMC}Py] =15 μM.

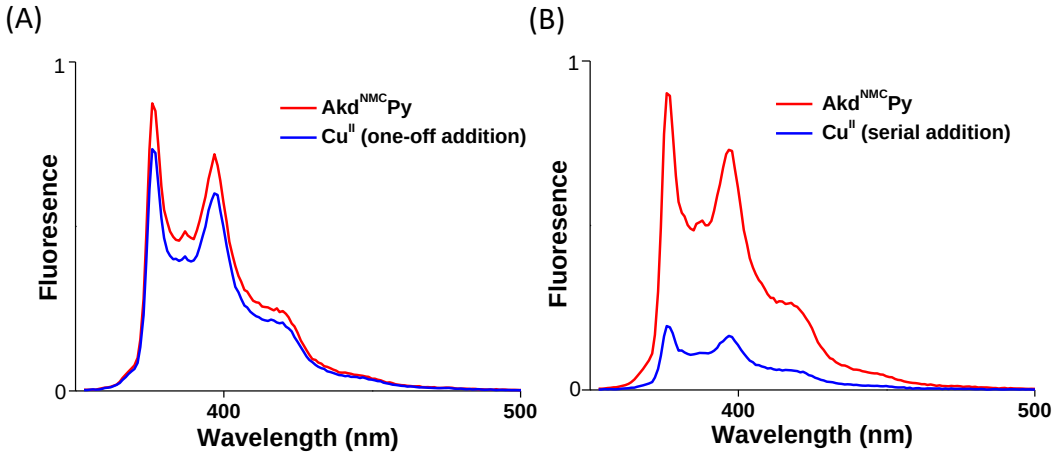

Fig. S3 Spectral changes during the one-off and serial addition of Cu^{II} into the Akd^{NMC}Py solution. (A) Fluorescence spectra after one-off addition of Cu^{II} (100 μM) in Akd^{NMC}Py (15 μM). (B) Fluorescence quenching after serial addition of Cu^{II} (100 μM) (Cu^{II} concentration increment is 5 μM each time of addition).

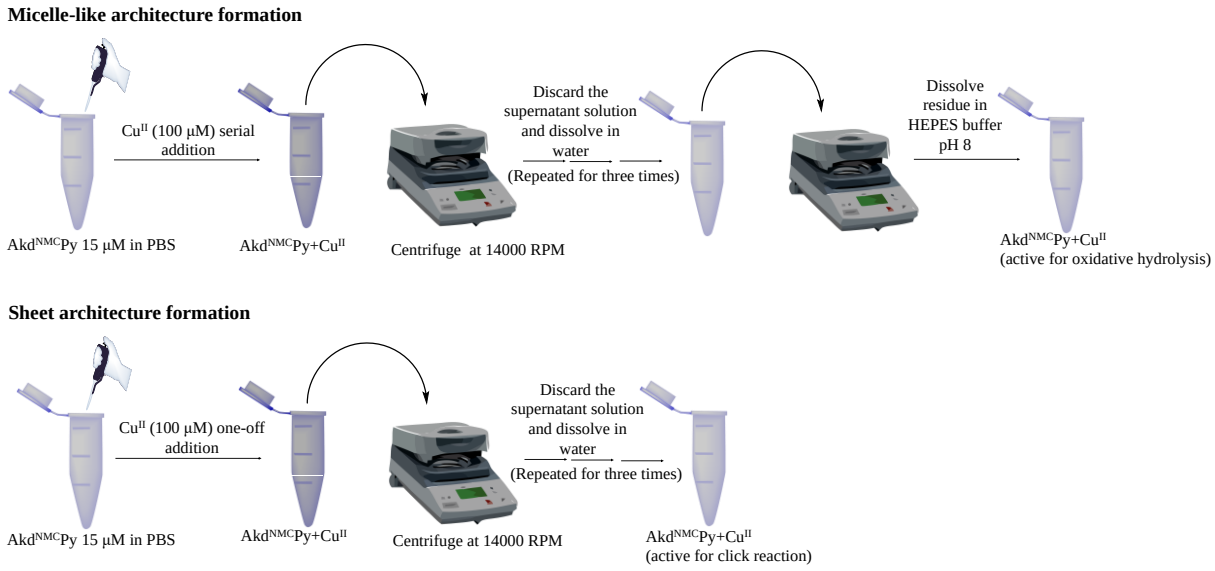

Fig. S4 Detailed experimental procedure for the micelle-like and sheet architectures formation.

$Akd^{NMC}Py$ with Cu^{II}	Excited state lifetime ($\lambda_{345\ nm}$)
$Akd^{NMC}Py$	140.8 ns
$Akd^{NMC}Py+Cu^{II}$ (1:1)	136.8 ns
$Akd^{NMC}Py+Cu^{II}$ (1:3)	121.5 ns
$Akd^{NMC}Py+Cu^{II}$ (1:5)	113.9 ns

Table S1 Excited-state lifetime experiment data of $Akd^{NMC}Py$ with Cu^{II} with varying concentration ratios.

(A) (B)

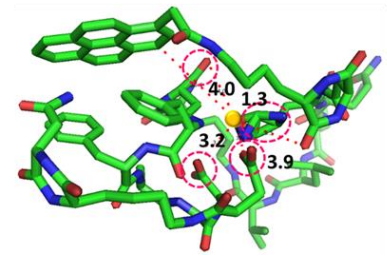

X	Distance (between Cu and X)
His (N)	1.3 Å
Kd (C terminus)(C=O)	4.0 Å
Kd (N terminus)(C=O)	5.5 Å
Py	6.6 Å
C=O (Glu)	3.9 Å
C=O (Asp)	3.2 Å

Fig. S5 (A) Most stable conformation of $Akd^{NMC}Py+Cu^{II}$. (B) Distance between Cu and different closer atoms (X) in $Akd^{NMC}Py$.

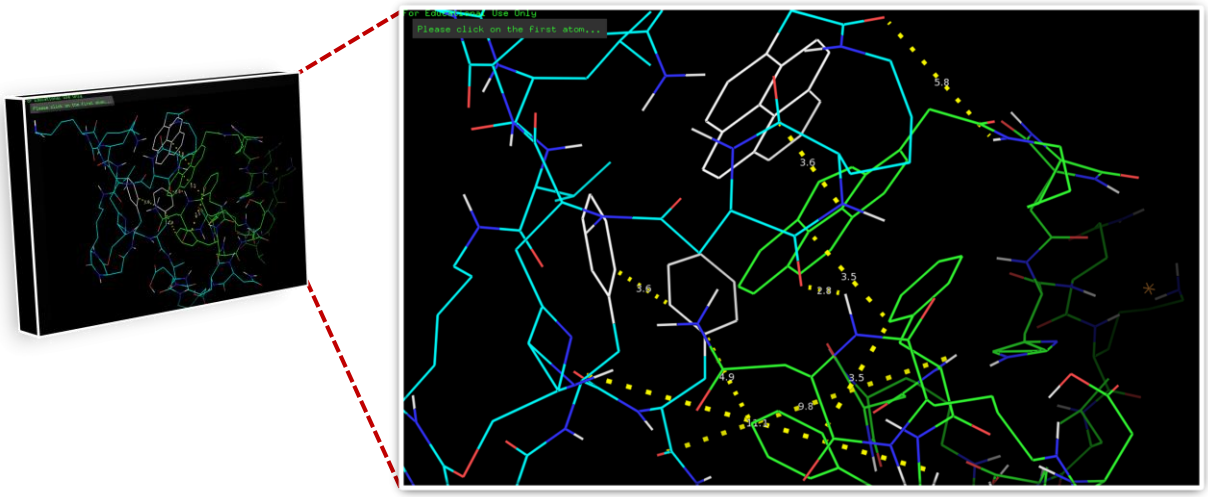

Akd^{NMC}Py-Copper motif	Akd^{NMC}Py motif	Type of interaction	Distance (Å)
Pyrene	Pyrene	intermolecular	3.8
Pyrene-Phe		intramolecular	3.5
Phe-Phe		intramolecular	3.5
	Phe-Phe	intramolecular	3.6
CDP (C-terminus)	CDP (N-terminus)	intermolecular	2.8
Pyrene amide	Pyrene amide	intermolecular	5.8
^{19}Phe amide	^{20}Phe amide	intermolecular	9.8
^{20}Phe amide	^{19}Phe amide	intermolecular	11.1

Fig. S6 Docking image of Akd^{NMC}Py in the pocket of Akd^{NMC}Py-Copper. Various molecular interactions, and their distances are listed in the table.

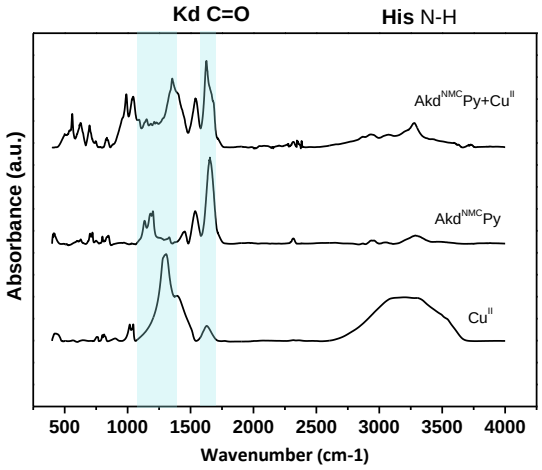

Fig. S7 FTIR spectra of (A) sheet structure of Akd^{NMC}Py with Cu^{II} (B) Akd^{NMC}Py, and (C) Cu^{II}. The data showed shifting of stretching frequencies of N-H (^{14}H) and -C=O (kd) in Akd^{NMC}Py from 3300 to 3275 cm^{-1} and 1654 to 1623 cm^{-1}, respectively, in the presence of Cu^{II} which suggest ^{14}H as the major binding site for Cu^{II}.

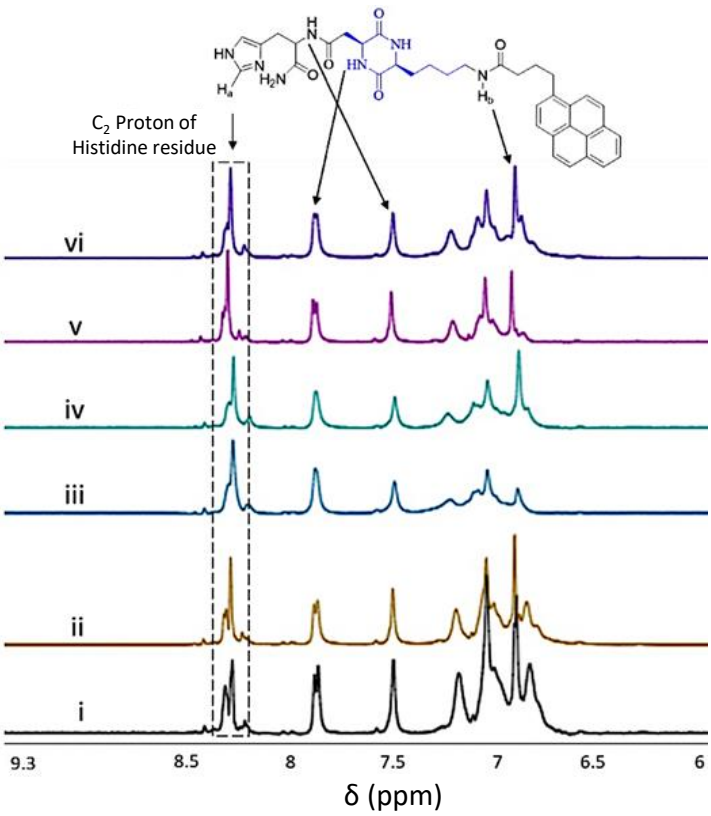

Fig. S8 ^{1}H NMR titration of HkdPy with Cu^{II} in D_2O solution at 25 °C and at a pH of 7.4. Spectrum (i) HkdPy (30 μM) dissolved in phosphate buffered D_2O (pH 7.45); spectra ii to vi are for same solution with Cu^{II} (50 μM), incubation time point are as follows: ii, 2 h; iii, 18 h; iv, 28 h; v, 40 h; vi, 2 days. The downfield shift of C_2 proton of ^{14}H confirming the Cu^{II}–H ($Akd^{NMC}Py$) binding interactions.

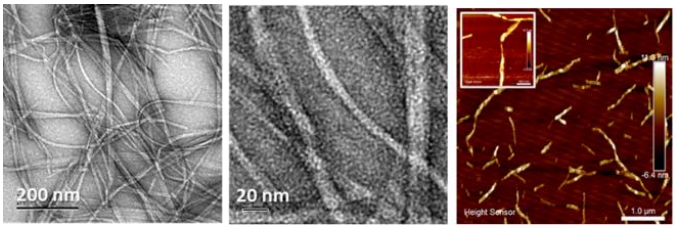

Fig. S9 TEM images of $Akd^{NMC}Py$ in PBS (pH 7.4) after 24 h incubation, form fibrillar architecture.

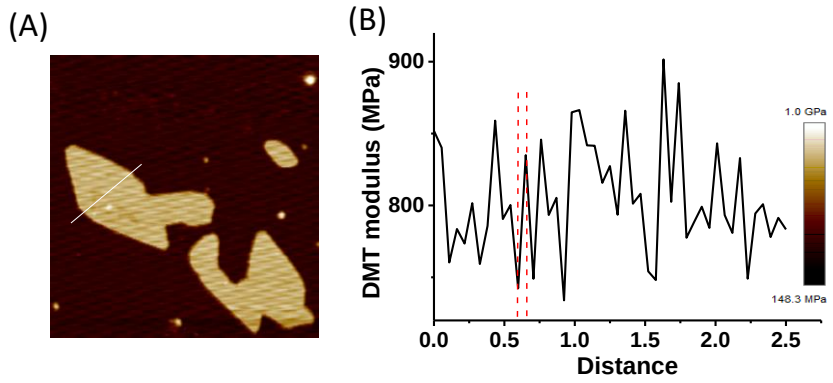

Fig. S10 A) AFM image of Akd^{NMC}Py+Cu^{I} (Sheets) in PBS (10 mM, pH 7.4). (B) DMT modulus plot of sheets.

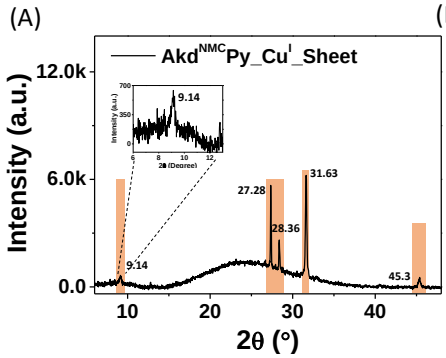

(B)

2θ	d_{hkl} (Å)
9.14	**9.5**
27.28	**3.5**
28.36	**3.4**
31.63	**2.9**
45.3	2.0

Fig. S11 (A) Powder XRD pattern and of nanosheet of Akd^{NMC}Py+Cu^{I}, (B) crystal lattice parameters 2θ and interplanar distances (dhkl). The π–π-stacking (Phe-Phe, Py-Py, Phe-Py) interactions (d-spacing: 3.5 and 3.4 Å), hydrogen bonding interactions of the peptide backbone to form a β-sheet packing (d-spacing: 9.5 Å), β-sheets hydrogen bonding connecting two adjacent CDPs (d-spacing: 2.9 Å).

Table S2 The time-dependent LC-MS of Akd^{NMC}Py+Cu$^{I/II}$ complex.

	Time (h)	Retention time (min)	Mass found (m/z)
i	0	7.8	Akd^{NMC}Py+3H^{+} (M/3= 717) Akd^{NMC}Py+2H^{+} (M/2= 1076)
ii	6	7.8 14.8	Akd^{NMC}Py+3H^{+} (M/3= 717) Akd^{NMC}Py+2H^{+} (M/2= 1076) Akd^{NMC}Py+Cu^{II}+K^{+} (M/3= 749)
iii	24	14.8	Akd^{NMC}Py+Cu^{II}+K^{+} (M/3= 749)

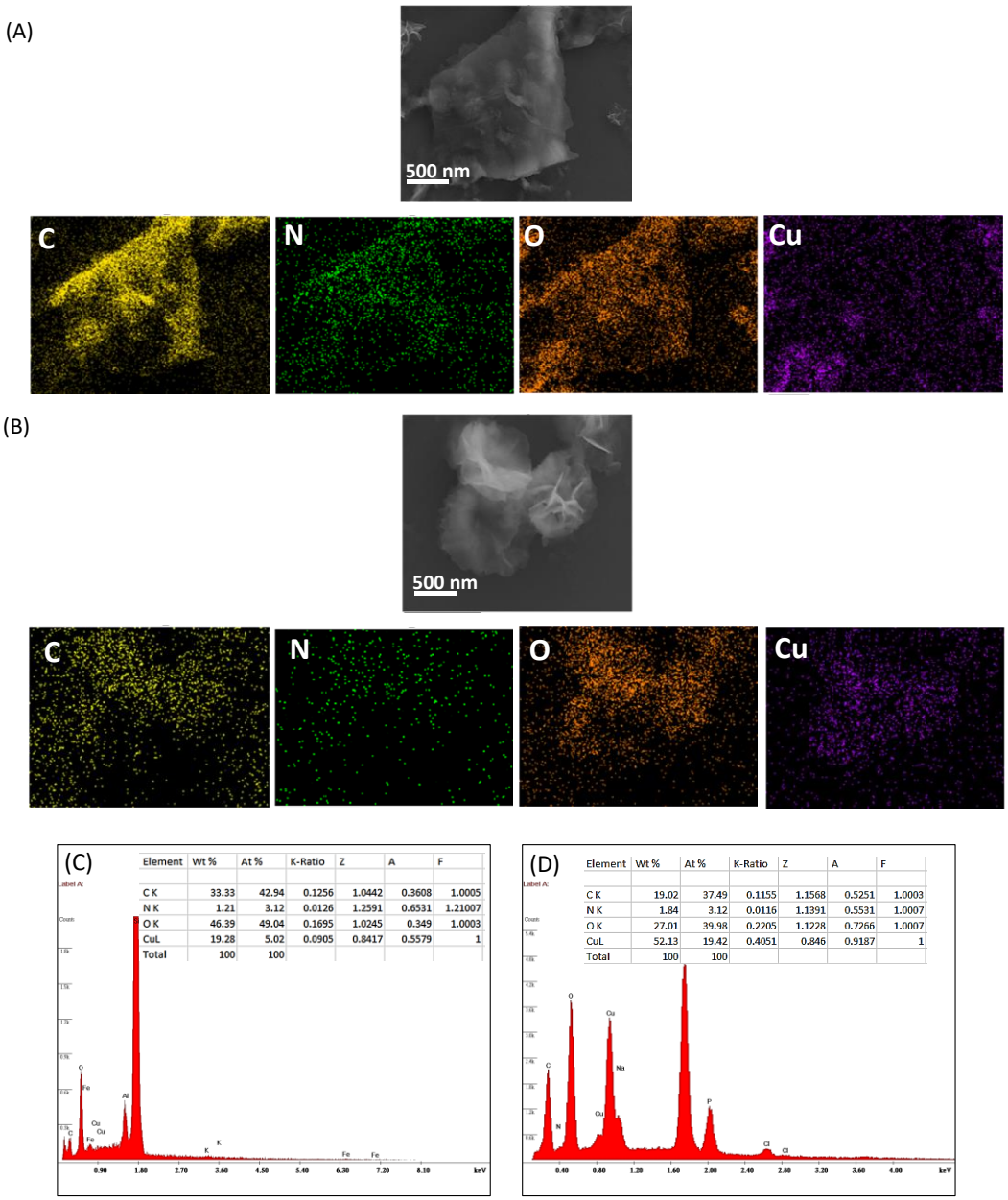

Fig. S12 FESEM images of Akd^{NMC}Py+Cu^{II}. (A) sheet (B) micelle-like architectures and corresponding elemental mapping images. EDAX ZAF quantification (Element Normalized) of (C) sheet (D) micelle-like architectures. The micelle-like architecture contains higher Cu content (wt% 52.13) compared to nanosheets (wt% 19.28).

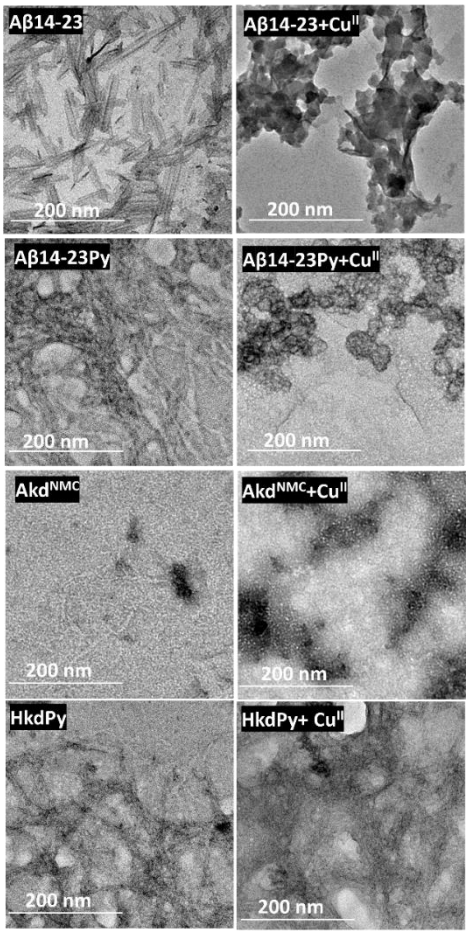

Fig. S13 TEM images of Aβ14-23, Aβ14-23Py, Akd^{NMC}, HkdPy and in the presence of Cu^{II} in PBS (pH 7.4). The data did not show sheet or micelle-like architectures upon prolonged incubation time.

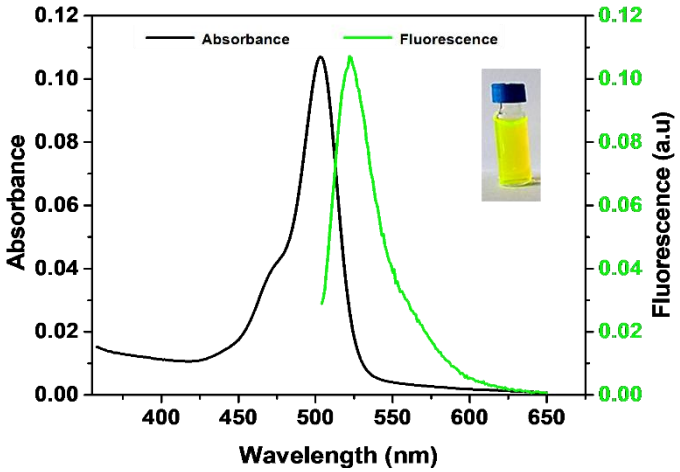

Fig. S14 Absorbance (λ_{max} = 504 nm) of DCFHDA and fluorescence (λ_{em} = 520 nm) spectra of DCF in the presence of micelle-like architectures of Akd^{NMC}Py+Cu^{II}.

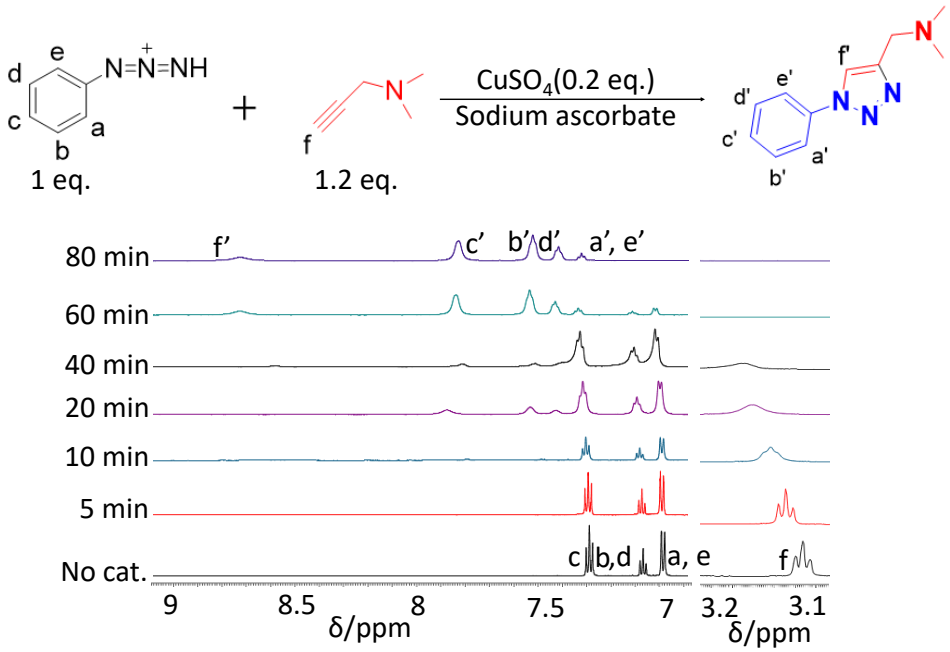

Fig. S15 Time-dependent ^{1}H-NMR spectra of reaction between phenyl azide (1 eq.) and *N*,*N*-dimethylprop-2-yn-1-amine (1.2 eq.) in the presence of $CuSO_4$+sodium ascorbate (0.2 eq.) added at 0 min and the product formation was assessed. $CuSO_4$+sodium ascorbate added at 0 min and product formation was observed within 20 min and reaction was completed 80 min.

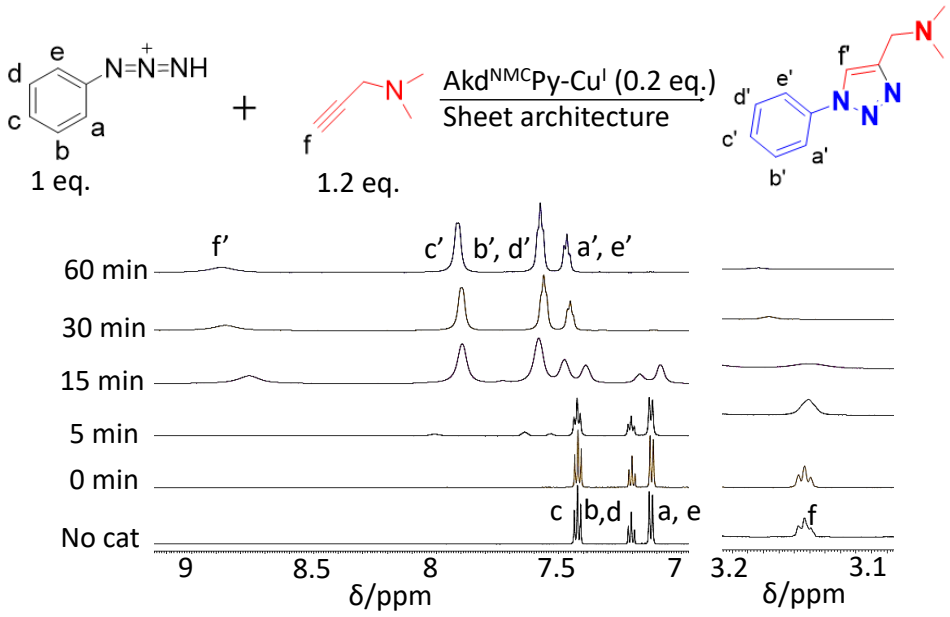

Fig. S16 Time-dependent ^{1}H-NMR spectra of the reaction between phenyl azide (1 eq.) and *N*,*N*-dimethylprop-2-yn-1-amine (1.2 eq.) in the presence of catalytic nanoarchitectures of $Akd^{NMC}Py+Cu^{I}$ (0.2 eq.). $Akd^{NMC}Py+Cu^{I}$ added at 0 min and product formation was observed within 10 min and reaction was almost completed in 30 min.

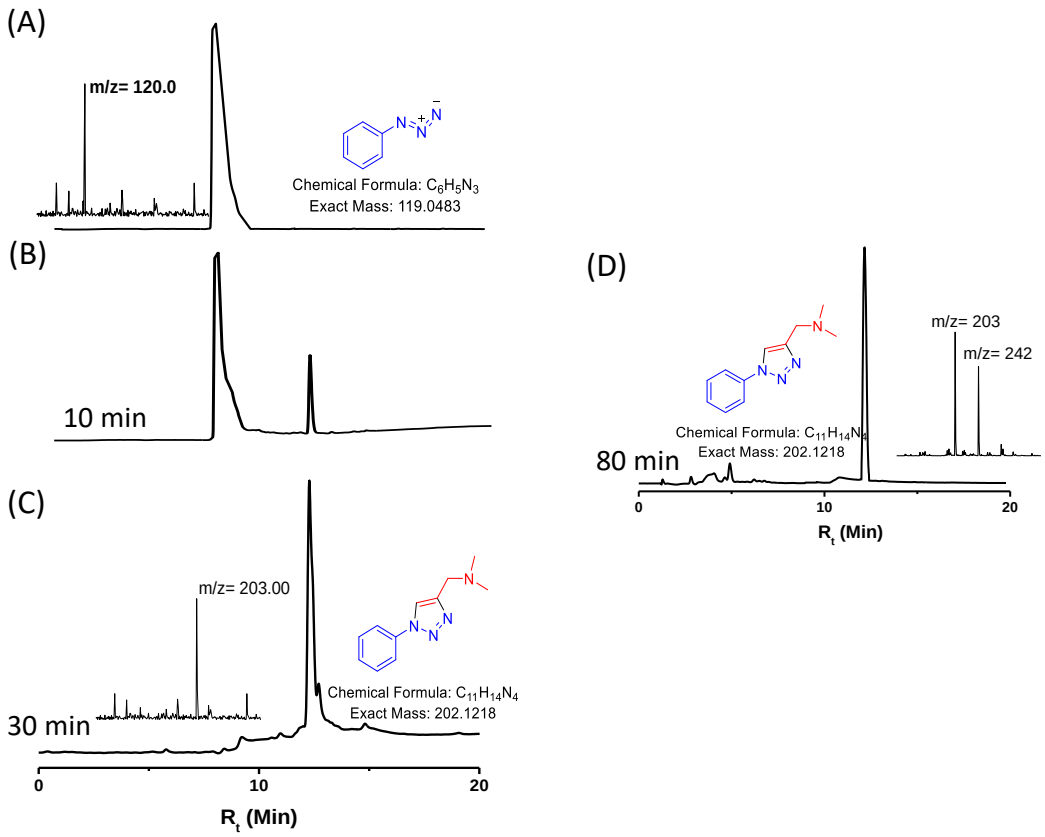

Fig. S17 The triazole product conversion was monitored using LC-MS. (A) LCMS of only phenyl azide (R_t=8.2 min). (B) Akd^{NMC}Py-Cu^{I} catalyzed alkyne-azide reaction (10% product triazole product, R_t= 13.0 min, m/z=203) after 10 min, (C) 97% triazole product was observed at 30 min, (D) LCMS profile of $CuSO_4$+sodium ascorbate catalyzed alkyne-azide reaction after 80 min showed 95% triazole product.

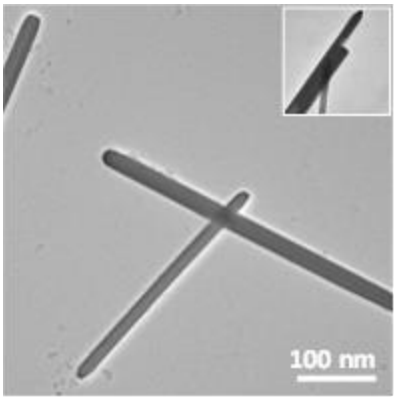

Fig. S18 One-off addition of Cu^{I} ($CuSO_4$+sodium ascorbate) into Akd^{NMC}Py generated nanorod architectures.

Table. S3 Comparison of the artificial hydrolase (oxidative-hydrolysis)

References	Artificial Hydrolase	Substrate	k_{cat}/K_m	Condition
Korendovych [4]	Ac-IHIHIYI-NH_2+Cu^{II}	DCFH-DA	61.2 (k_2 M^{-1} min^{-1})	HEPES (pH 8)
Our work	**$Akd^{NMC}Py$+Cu^{II}**	**DCFH-DA**	**120.96 ($M^{-1}min^{-1}$)**	**HEPES (pH 8)**

Table S4 Mass (MS) profiles of triazole products.

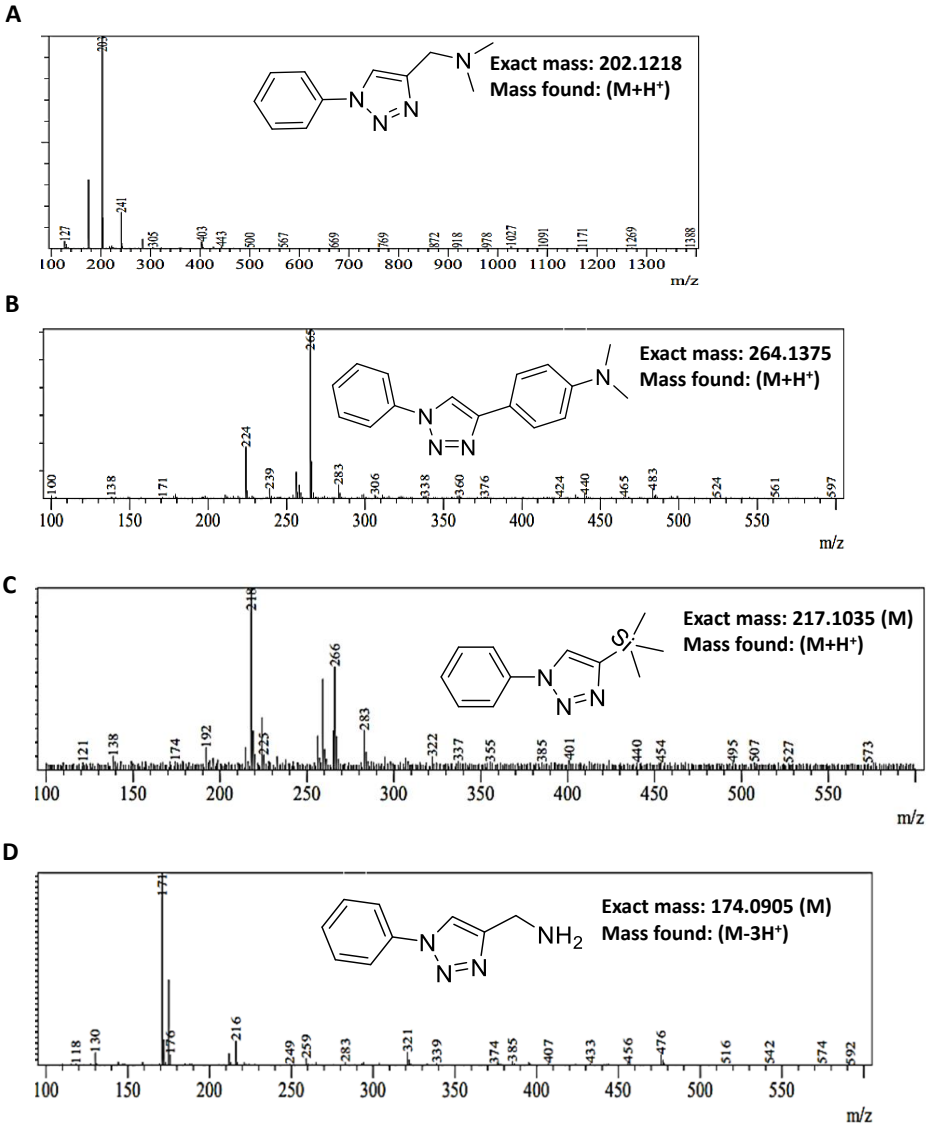

Table S5 Characterizations of the peptidomimetics by HRMS and HPLC.

Name	Sequence	Exact mass	Observed mass HRMS
Aβ14-23	His-Gln-Lys-Leu-Val-Phe-Phe -Ala-Glu-Asp	1231.6350	616.8319 $[M/2+H]^+$
Aβ14-23Py	Py-His-Gln-Lys-Leu-Val-Phe-Phe-Ala-Glu-Asp	1473.7081	737.8486 $[M/2+H]^+$
Akd^{NMC}	kd- His-Gln-Lys-Leu-Val-kd-Phe-Phe-Ala-Glu-Asp-kd	1906.9690	954.9907 $[M/2+H]^+$
$Akd^{NMC}Py$	Py-kd- His-Gln-Lys-Leu-Val-kd-Phe-Phe-Ala-Glu-Asp-kd	2149.0421	1076.0255 $[M/2+H]^+$ 717.687 $[M/3+H]^+$
HkdPy	Py-kd-His	649.3012	650.3004 $[M+H]^+$

Peptide/ peptidomimetics	HPLC Gradient	Flow rate (ml/min)	Retention time (Rt)	Purity (%)
Aβ14-23	0-98 % MeCN (0.1% TFA) in H_2O (0.1% TFA) for 25 min	8	10.1 min	>99
Aβ14-23Py	0-98 % MeCN (0.1% TFA) in H_2O (0.1% TFA) for 25 min	8	12.8 min	>99
Akd^{NMC}	0-98 % MeCN (0.1% TFA) in H_2O (0.1% TFA) for 25 min	8	10.2 min	>99
$Akd^{NMC}Py$	0-98 % MeCN (0.1% TFA) in H_2O (0.1% TFA) for 25 min	8	13.0 min	>99

HPLC Chromatogram and HRMS data of Aβ14-23

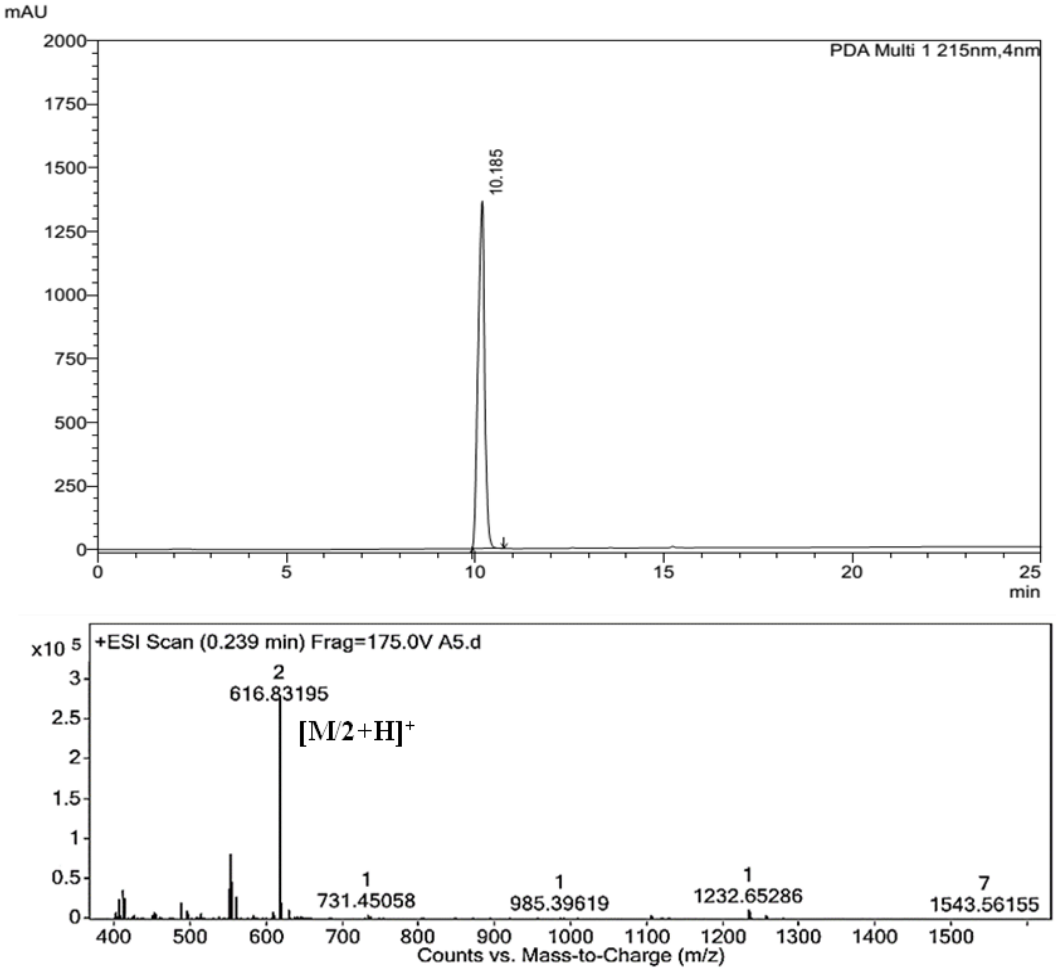

HPLC Chromatogram and HRMS data of Aβ14-23Py

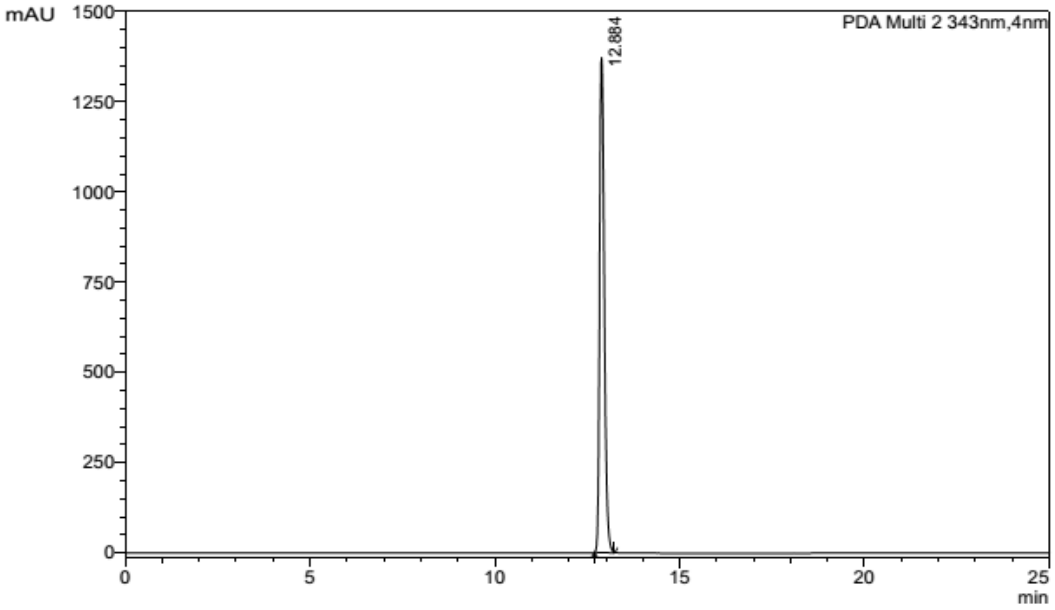

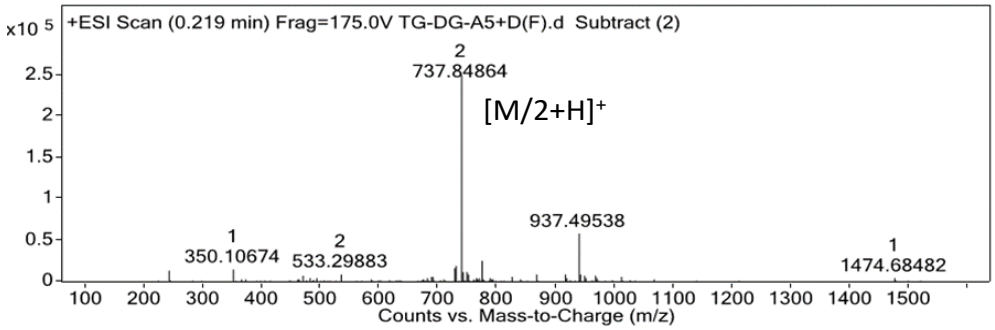

HPLC Chromatogram and HRMS data of Akd^{NMC}

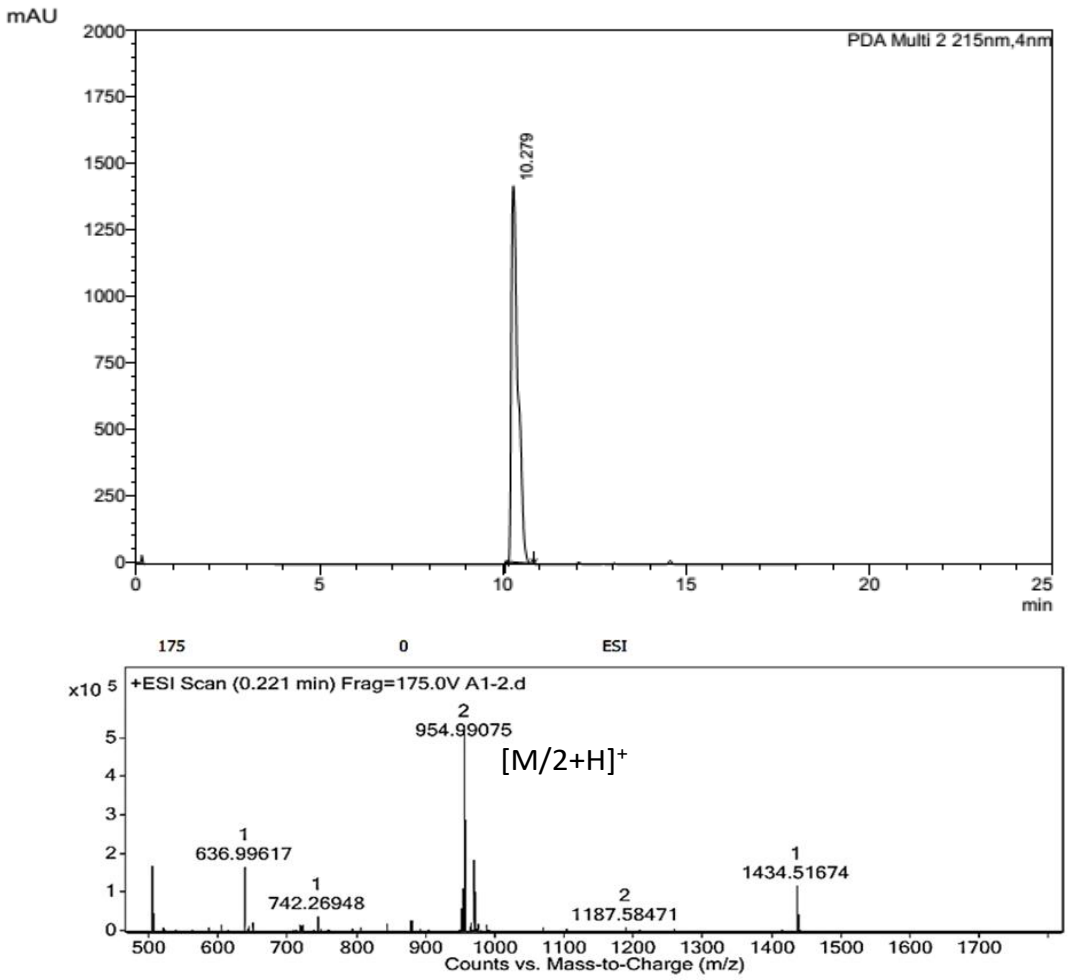

HPLC Chromatogram and HRMS data of Akd^{NMC}Py

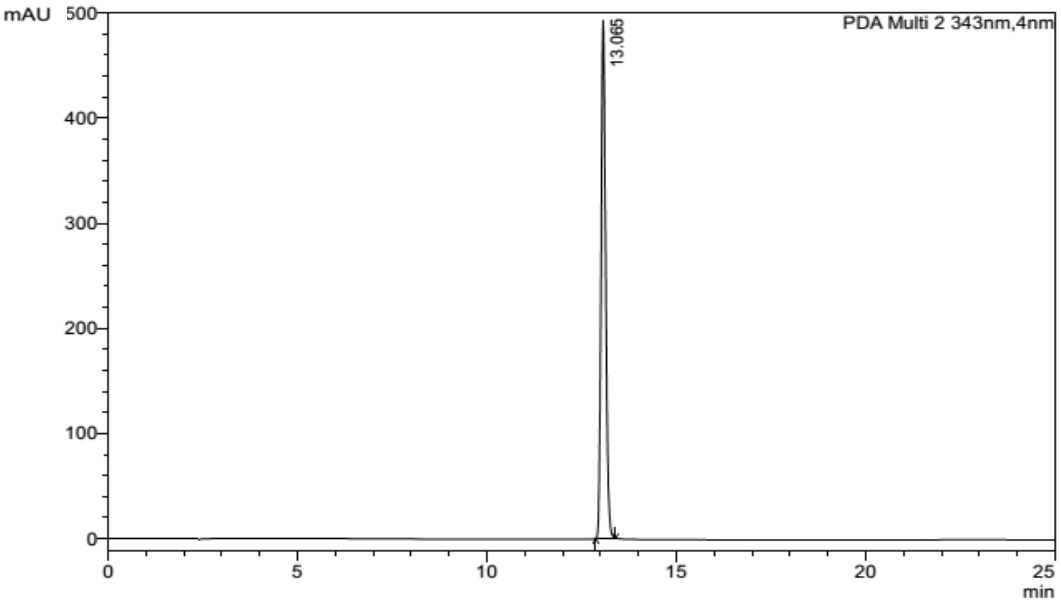

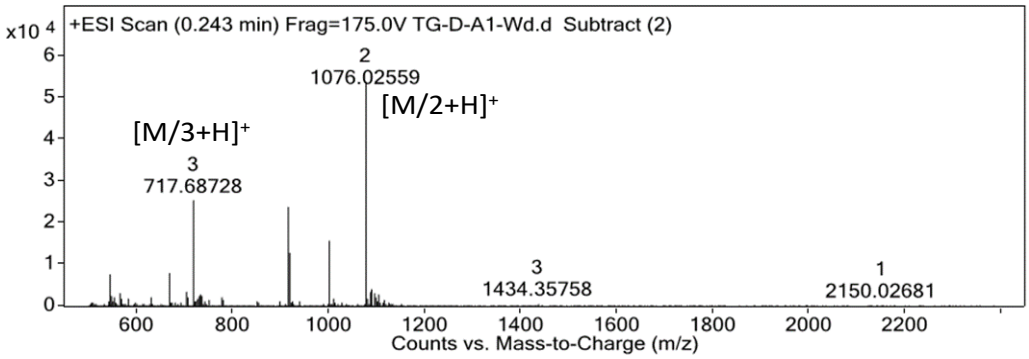

^{1}H NMR and LCMS of HkdPy

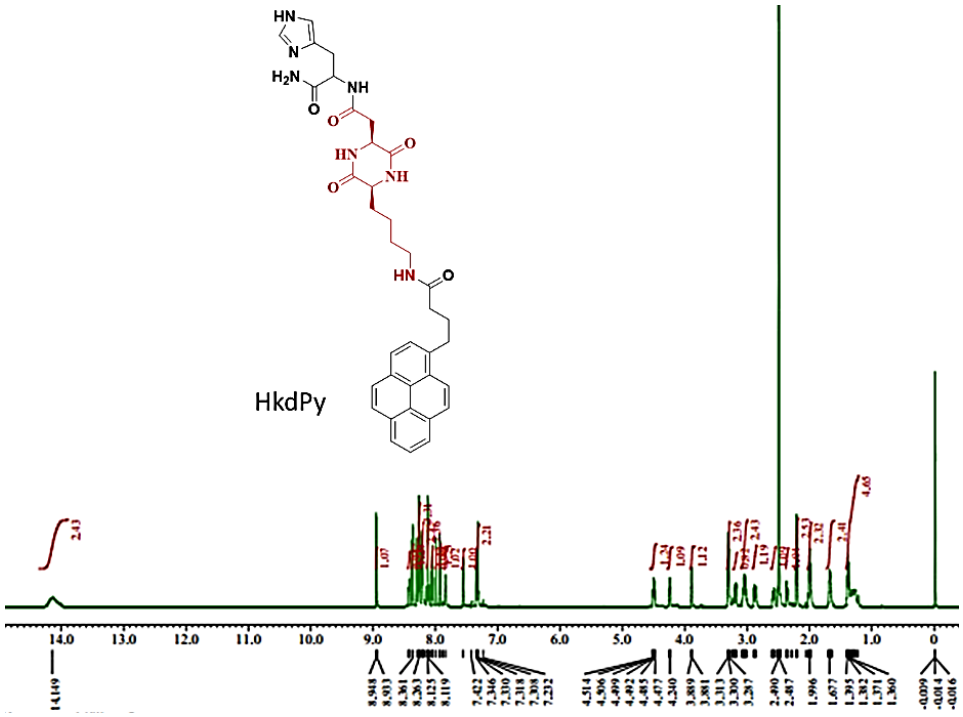

LC

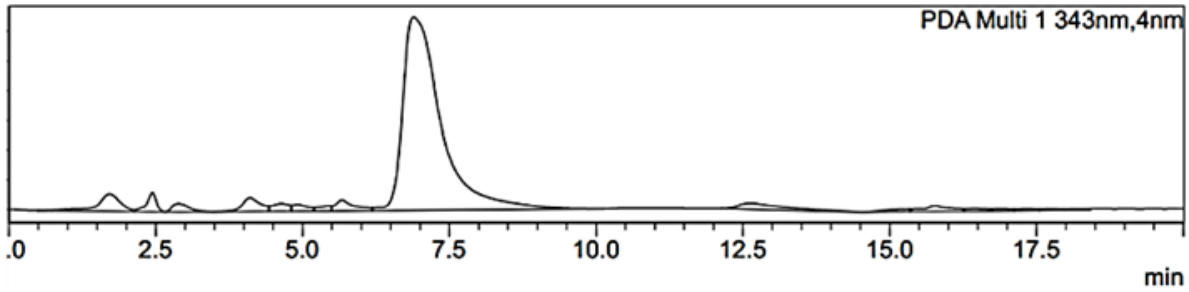

MS

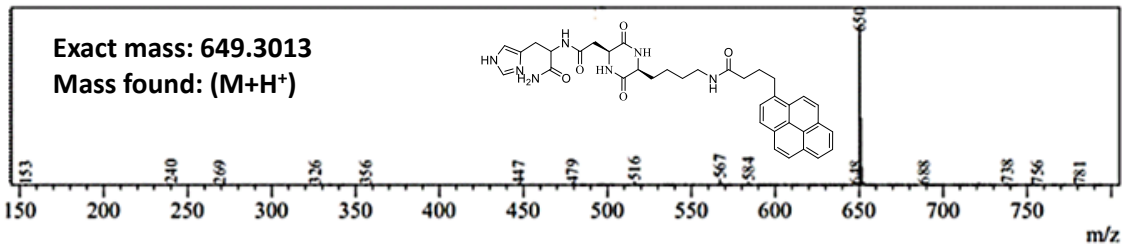

5. References

[1] C. Madhu, C. Voshavar, K. Rajasekhar, T. Govindaraju, *Org. Biomol. Chem.,* 2017, **15**, 3170-74.
[2] M. Konar, D. Ghosh, S. Smanata, T. Govindaraju, *RSC Chem. Biol.,* 2022*, DOI: 10.1039/d1cb00235j*
[3] D. Piovesan, G. Minervini, S. C. Tosatto, *Nucleic Acids Res.,* 2016, **44**, W367-W74.
[4] Z, Lengyel, C. M. Rufo, Y. S. Moroz, O. V. Makhlynets, I. V. Korendovych, *ACS Catal.,* 2018, **8**, 59-62.